Geochemical Perspectives Letters



# Solar neon dissolution into an ultramafic magma ocean

C.D. Cardoso[1*], M. Moreira[1], B. Scaillet[1]

OPEN ACCESS

https://doi.org/10.7185/geochemlet.2520

## Abstract

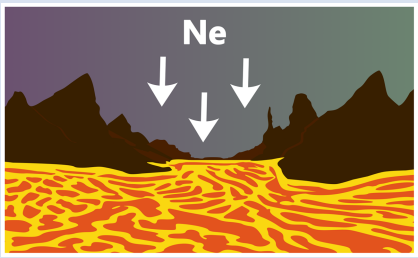


The solar-like neon isotopic signature of the mantle suggests the presence of a primitive reservoir. Its origin remains a puzzle, though the literature suggests that a primordial $H_2$ and He-rich atmosphere captured from the accretion disk was dissolved into a magma ocean. Our study investigates how much neon can be incorporated into the magma ocean based on the basal pressure of such an atmosphere and the neon solubility in mafic to ultramafic melts (49–34 wt. % $SiO_2$ and 9–21 wt. % MgO). The neon solubility range obtained ($3.4 \times 10^{-4}$ to $6.5 \times 10^{-5}$ cm$^3$ STP g$^{-1}$ bar$^{-1}$) cannot match the primitive mantle theoretical neon content in a slow accretion scenario, demanding either fast accretion or alternative models for neon origin on Earth. Considering the planetary embryo mass required to accumulate enough neon (>0.8 times the mass of the Earth), the hypothesis of partial dissolution of the atmosphere into the magma ocean remains difficult to consider.

Received 19 December 2024 | Accepted 6 May 2025 | Published 12 June 2025

## Introduction

Establishing the source of deep mantle Ne is key to understanding the formation of Earth and its primitive atmosphere. The $^{20}Ne/^{22}Ne$ of the deep mantle (up to $13.03 \pm 0.04$; Williams and Mukhopadhyay, 2019) approaches that of solar wind ($13.36 \pm 0.10$; Heber *et al.*, 2012); if we consider isotopic fractionation to be limited, then this signature points to the presence of a primitive reservoir, as is the case for helium isotopes (*e.g.*, Kurz *et al.*, 1982). The origin of this solar neon has been assigned to partial dissolution of a solar-like atmosphere ($H_2$ and He-rich) from the accretion disk into the magma ocean (*e.g.*, Mizuno *et al.*, 1980; Yokochi and Marty, 2004). However, Jaupart *et al.* (2017) and Olson and Sharp (2019) demonstrated that this model only dissolves enough neon if the mass of the proto-Earth is adequate (>0.2–0.3 times the mass of the Earth—$M_{Earth}$) to sustain dense atmospheres. Additionally, the gas from the accretion disk is only present, at most, in the first 10 Myr of planetary formation (*e.g.*, Williams and Cieza, 2011), when the mass of the protoplanet is modelled to be below 0.2 $M_{Earth}$ in the distance from the sun where the Earth was formed (Walsh and Levison, 2016; Jaupart *et al.*, 2017). The captured atmosphere scenario is thus only possible if there was fast accretion, allowing a higher mass and hence higher atmospheric pressure and ingassing.

In the Jaupart *et al.* (2017) model, they employed the solubility of neon in tholeiitic basalts to establish the amount of neon that could be trapped in the magma ocean from the simulated atmospheric conditions. Olson and Sharp (2018) demonstrated that gas solubility is a critical parameter in establishing the volatile abundances in the magma ocean phase. In this paper, we present new neon solubility values for a range of silica (49 to 34 wt. %) and MgO (9 to 21 wt. %) contents, and update the Jaupart *et al.* (2017) model by approaching the early Earth magma ocean composition, which we assume to resemble the theoretical pyrolite composition (~45 wt. % $SiO_2$ and ~39 wt. % MgO; Lyubetskaya and Korenaga, 2007).

## Material and Methods

Experiments were performed on a natural tholeiitic basalt glass mixed with various fractions of a $MgO:Fe_2O_4$ mixture (1:1.25) to approach ultramafic compositions. The powder was melted at 1400 °C for 3 hr in an open Pt crucible. The resulting dry glass used on the experiments was grinded (<200 µm) in an agate mortar under acetone. The starting dry glass shows homogeneous composition (Table 1). Each experimental run was done with 0.3 (EXP01 and EXP02) or 1 g of sample loaded in an open Pt crucible in a horizontal furnace permanently flushed with 1 bar of neon gas, and left for at least 3 hr under ~1400 °C. The experiments were ended by removing the Pt crucible and dropping it in water; experiment duration and the composition of glasses are in Tables 1 and 2. During the experiments, the gas was introduced via tubes into a closed system ending in a water container in order to flush out the air and prevent atmospheric contamination. Our gas is composed of pure neon and our procedure follows that of Jambon *et al.* (1986), who demonstrated that gas composition (*i.e.* whether pure Ne or mixed with other gases), pressure and experiment duration do not substantially affect the neon solubility in basaltic glasses, which follows Henry's law under the experimental conditions investigated here. We conclude that the neon contents we report are representative of the solubility of the compositions of interest. Grain images to detect the presence or not of bubbles and crystals were obtained using an SEM-EDS under 15 kV accelerating voltage, 60 µm aperture, and at 10 mm working distance; images are

1. Institut des Sciences de la Terre d'Orléans, UMR 7327, Université d'Orléans-CNRS, Orléans, France
* Corresponding author (email: carolina.dantas-cardoso@univ-orleans.fr)

**Table 1** Composition of the starting dry glass and experimental glasses (wt. %). "*n*" refers to the number of analyses per sample.

| Sample (*n*) | $SiO_2$ | $TiO_2$ | $Al_2O_3$ | FeO | MnO | MgO | CaO | $Na_2O$ | $K_2O$ | Total |
|---|---|---|---|---|---|---|---|---|---|---|
| *Starting dry glass* | | | | | | | | | | |
| CH31-DR12 (10) | 49.90 | 1.28 | 14.92 | 9.74 | 0.16 | 8.63 | 12.13 | 2.06 | 0.21 | 99.01 |
| σ | 0.32 | 0.09 | 0.23 | 0.26 | 0.05 | 0.04 | 0.09 | 0.06 | 0.05 | |
| *Experimental glass* | | | | | | | | | | |
| EXP01 (12) | 48.60 | 1.22 | 14.81 | 13.22 | 0.17 | 8.63 | 11.84 | 1.04 | 0.11 | 99.65 |
| σ | 0.40 | 0.11 | 0.23 | 0.27 | 0.08 | 0.10 | 0.11 | 0.15 | 0.03 | |
| EXP02 (12) | 47.37 | 1.19 | 14.19 | 10.82 | 0.15 | 12.01 | 11.61 | 1.79 | 0.19 | 99.34 |
| σ | 0.32 | 0.12 | 0.14 | 0.18 | 0.07 | 0.10 | 0.11 | 0.04 | 0.05 | |
| EXP03 (15) | 46.19 | 1.16 | 13.73 | 13.59 | 0.13 | 11.77 | 11.28 | 1.83 | 0.17 | 99.86 |
| σ | 0.35 | 0.07 | 0.14 | 0.37 | 0.06 | 0.13 | 0.08 | 0.04 | 0.03 | |
| EXP04 (10) | 41.33 | 0.99 | 12.61 | 16.75 | 0.12 | 14.74 | 10.11 | 1.59 | 0.18 | 98.41 |
| σ | 0.32 | 0.07 | 0.24 | 0.40 | 0.08 | 0.21 | 0.06 | 0.06 | 0.03 | |
| EXP04B (12) | 42.10 | 1.06 | 12.48 | 17.30 | 0.12 | 14.96 | 10.31 | 1.66 | 0.16 | 100.16 |
| σ | 0.39 | 0.04 | 0.14 | 0.50 | 0.08 | 0.08 | 0.08 | 0.04 | 0.04 | |
| EXP05 (10) | 39.04 | 0.98 | 11.75 | 18.06 | 0.10 | 16.74 | 9.51 | 1.49 | 0.15 | 97.83 |
| σ | 0.35 | 0.10 | 0.14 | 0.63 | 0.07 | 0.12 | 0.09 | 0.05 | 0.05 | |
| EXP06 (12) | 35.07 | 0.87 | 10.50 | 22.68 | 0.10 | 19.59 | 8.76 | 1.42 | 0.18 | 99.17 |
| σ | 0.25 | 0.07 | 0.11 | 0.37 | 0.06 | 0.15 | 0.10 | 0.05 | 0.03 | |
| EXP06B (12) | 35.42 | 0.87 | 10.21 | 21.98 | 0.13 | 19.91 | 8.83 | 1.39 | 0.17 | 98.91 |
| σ | 0.47 | 0.10 | 0.26 | 0.71 | 0.08 | 0.34 | 0.34 | 0.07 | 0.04 | |
| EXP07 (10) | 33.77 | 0.81 | 9.75 | 24.06 | 0.14 | 20.77 | 8.84 | 1.40 | 0.14 | 99.69 |
| σ | | 0.19 | 0.09 | 0.11 | 0.54 | 0.06 | 0.18 | 0.07 | 0.02 | 0.03 |

**Table 2** $^{22}Ne$ solubility results obtained from 5 grains including the temperature and duration of each experiment performed at 1 bar.

| Sample | *T* (°C) | duration (hr) | $^{22}Ne$ solubility ($\times 10^{-4}$ cm$^3$ STP g$^{-1}$ bar$^{-1}$) | σ ($\times 10^{-4}$) | $^{22}Ne$ solubility ($\times 10^{-5}$ wt. % bar$^{1}$) |
|---|---|---|---|---|---|
| EXP01 | 1400 | 24 | 3.36 | 0.26 | 3.02 |
| EXP02 | 1400 | 24 | 2.92 | 0.36 | 2.62 |
| EXP03 | 1345 | 4 | 1.94 | 0.26 | 1.75 |
| EXP04 | 1400 | 4 | 1.71 | 0.25 | 1.54 |
| EXP04B | 1400 | 3 | 1.76 | 0.08 | 1.58 |
| EXP05 | 1400 | 4 | 1.50 | 0.08 | 1.35 |
| EXP06 | 1400 | 2 | 0.95 | 0.13 | 0.86 |
| EXP06B | 1400 | 3 | 0.90 | 0.10 | 0.81 |
| EXP07* | 1400 | 4 | 0.65 | 0.06 | 0.59 |

included in the Supplementary Information. Chemical composition was obtained with a Cameca SX-Five electron microprobe under an accelerating voltage of 15 kV, a beam current of 10 nA, counting times of 10 seconds per element and a defocused beam diameter of 20 µm to minimise alkali migration. The calibration of major elements was performed using the following standards: albite (Si, Na), $TiMnO_3$ (Mn, Ti), $Al_2O_3$ (Al), FeO (Fe), MgO (Mg), orthoclase (K), andradite (Ca) and apatite (P). PET analyser crystals were used for elements with lower energy emissions (K, Ti, P and Ca), while LiF analyser crystals were employed for higher energy emissions (Fe and Mn) (Di Carlo *et al.*, 2006). Five grains of each resulting glass composition were heated, using a laser type Ytterbium-doped fibre ($T > 1500$ °C), analysed on a quadrupole mass spectrometer (QMS 700) and showed a small standard deviation (4 to 15 %; Table 2) with blanks contributing up to 1.6 % to the $^{22}Ne$ abundance. All procedures were undertaken at the Institut des Sciences de la Terre d'Orléans (ISTO). Homogeneous chemical composition and neon content in different grains along with the absence of bubbles confirm that equilibrium was reached. The fact that the Ne solubility data of the most viscous liquid of our series (basalt) is similar to that of previous studies (see below) shows that the role of bubbles, which would be made of pure Ne and thus strongly increase Ne bulk content, is minor to non-existent.

## Neon Solubility in Ultramafic Melts

As a noble gas, Ne is chemically inert and thus solubility is not controlled by chemical processes but by weak van der Waals interactions between the atoms and the silicate melt. The size of the atoms is the main parameter in this type of physical solubility (*e.g.*, Doremus, 1966), or ionic porosity (*e.g.*, Carroll and Stolper, 1993), with lighter noble gases displaying higher solubility than heavier ones (*e.g.*, Jambon *et al.*, 1986). The quantity of noble gas dissolved in the melt is controlled by the partial

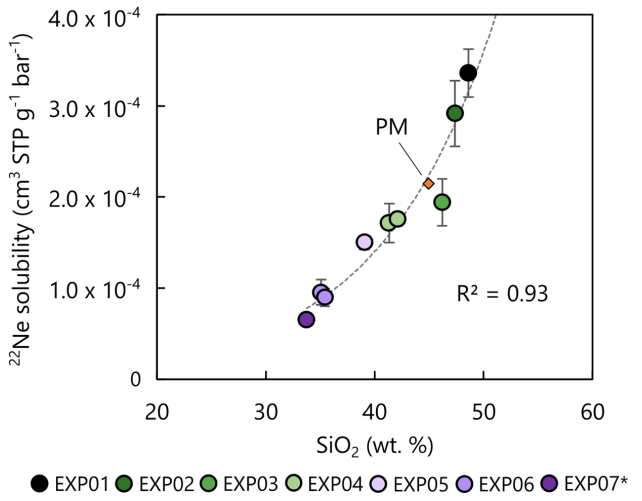


**Figure 1** Experimental results (1400 °C, 1 bar of Ne) with best fit (Eq. 1) and expected solubility value for the primitive mantle (PM; Lyubetskaya and Korenaga, 2007). Error bars represent the standard deviation. *Result for the 72 % glass phase. The dashed line represents the model equation (1) discussed in the text.

pressure of said gas, following Henry's law. Experimental studies demonstrated that neon solubility is higher in rhyolites than in basalts (*e.g.*, Carroll *et al.*, 1994), possibly due to the available space between $SiO_2$ tetrahedra links (Shackelford *et al.*, 1972). Our results are in agreement with this hypothesis, as $^{22}Ne$ solubility decreases with $SiO_2$ contents, from $3.4 \times 10^{-4}$ cm$^3$ STP g$^{-1}$ bar$^{-1}$ in a tholeiitic basalt (49 wt. % $SiO_2$ and 9 wt. % MgO) to as low as $6.5 \times 10^{-5}$ cm$^3$ STP g$^{-1}$ bar$^{-1}$ in ultramafic rocks (34 wt. % $SiO_2$ and 21 wt. % MgO) (Table 1 and Table 2, Fig. 1). The resulting glasses showed minimal compositional variation and presence of bubbles (<10 μm), with limited and localised quenched crystals (EXP06B, Fig. S-1). Only the experiment with lowest $SiO_2$ content (34 wt. %) produced crystals in equilibrium (EXP07, Fig. S-2). The neon solubility of this experiment is an estimation from the glass phase based on a least square mass balance calculation (Albarède, 1996) between the three phases produced during the experiment: glass (~72 wt. %), olivine (~16 wt. %) and spinel (~12 wt. %) crystals. Our result for the tholeiitic basalt is compatible with the literature (~2.5 to $3.5 \times 10^{-4}$ cm$^3$ STP g$^{-1}$ bar$^{-1}$ from 49 to 50 wt. %; Jambon *et al.*, 1986; Lux, 1987; Iacono-Marziano *et al.*, 2010), whereas the results from our experimental ultramafic compositions fall above the estimates of the Iacono-Marziano *et al.* (2010) model, which yields values as low as $6 \times 10^{-5}$ cm$^3$ STP g$^{-1}$ bar$^{-1}$. This difference is likely due to the fact that, although $SiO_2$ content is the main factor in the ionic porosity, the introduction of network modifiers cations, such as MgO, can further reduce the interstitial space and thus noble gas atoms are not accommodated (Shibata *et al.*, 1998). For simplification, the primitive mantle composition (PM) we refer to in our model is only based on the $SiO_2$ content (45 wt. %). From the experimental data, we obtain the best fit for $^{22}Ne$ solubility ($s$) based on the $SiO_2$ content ($R^2 = 0.93$):

$$s = 3.22 \times 10^{-6} e^{9.43 \times 10^{-2} SiO_2} \quad \text{Eq. 1}$$

## Neon Concentration in the Magma Ocean

Rough estimates of the current $^{22}Ne$ content in the upper mantle are ~$10^{-11}$ cm$^3$ STP g$^{-1}$ (Moreira and Kurz, 2013) (~$10^{-8}$ ppm). Considering that over 99 % of the volatiles degassed from the mantle (*e.g.*, Allègre *et al.*, 1986), the primitive mantle composition would approach at least $10^{-9}$ cm$^3$ STP g$^{-1}$ for $^{22}Ne$ (~$10^{-6}$ ppm). Starting with the Jaupart *et al.* (2017) accretion model, we can establish the amount of neon that can be captured from the primitive atmosphere. In this model, the atmosphere symmetrically surrounds the embryo following the Bondi radius, *i.e.* the region around the embryo that is able to attract gas and dust particles. We modified this model by removing the luminosity, as it showed minimal influence, and applied an upper bound nebula photoevaporation range of 10 Myr, as some models show the nebula dissipating before 8 Myr (*e.g.*, Ercolano and Pascucci, 2017), especially if we only consider the inner solar system and not the whole disk. With our new values of neon solubility, even lower concentrations are obtained for a melt with 30 to 49 wt. % $SiO_2$. For the theoretical pyrolite composition of ~45 wt. % $SiO_2$ (Lyubetskaya and Korenaga, 2007), $^{22}Ne$ solubility would be close to $2 \times 10^{-4}$ cm$^3$ STP g$^{-1}$ bar$^{-1}$ based on EXP03 (Table 2) and Equation 1, yielding ~$10^{-11}$ cm$^3$ STP g$^{-1}$ of dissolved $^{22}Ne$ for a 0.2 $M_{Earth}$ embryo with $2.0 \times 10^{-3}$ bar atmosphere and ~$1.5 \times 10^{-7}$ bar $^{22}Ne$ partial pressure. Our ranges are lower than the ones from Jaupart *et al.* (2017), and thus even less compatible with the $^{22}Ne$ content estimations for the primitive mantle. As seen in Figure 2b, only embryos with over 0.8 $M_{Earth}$ are capable of capturing enough neon in the magma ocean to reflect the primitive mantle composition.

Our model can be contested on the basis of whether or not Earth accretion took place in a faster pace, allowing for >0.2 $M_{Earth}$ to be formed still in the presence of the solar nebula. If accretion was slow (*e.g.*, ~30 Myr or more to achieve 90 % of the mass), the nebula gas could not be captured as the mass would be too low, as would the surface pressure. There is still debate whether Earth's accretion took place in the first 10 Myr or if it extended to ~30 Myr, or more. Hf-W isotopes yield different core formation ages depending on the model applied; however, according to certain authors (*e.g.*, Halliday *et al.*, 1996; Kleine and Walker, 2017), the two-stage model (~30 Myr; *e.g.*, Kleine and Walker, 2017) represents the earliest age of core formation. Nonetheless, it is possible that most of the core was formed in the early stages of accretion but extended beyond the age of Mars accretion, for instance, based on mantle $^{182}W$ isotopes (Kleine and Walker, 2017). Yin *et al.* (2002) proposed a model with exponential decrease in accretion and previous metal–silicate equilibrium with the magma ocean before segregation to the core; they obtained 63 % core formation by 11 Myr and 90 % by 29 Myr. Several growth models agree that Mars analogues are formed in a few Myr (*e.g.*, Walsh and Levison, 2016); however, the question remains open for Earth-like bodies.

In the Olson and Sharp (2019) fast accretion model (up to 16 Myr), the surface pressure and temperature continually increase until 50 % of the accretion and then starts to drop. The magma volatiles content, however, stays relatively stable after this mark, when the solar nebula would be nearly fully dissipated (up to 10 Myr). Nonetheless, applying the Jaupart *et al.* (2017) model for an embryo of 0.5 $M_{Earth}$ (under ~$5 \times 10^{-2}$ bar, Fig. 2a), it would still not reach the primitive mantle estimate, especially for the lower silica-rich compositions (Fig. 2b). Considering that our model yields an upper bound for neon concentration, as mantle equilibration is not assured, the atmosphere capture into the magma ocean scenario remains improbable. Furthermore, if the magma ocean was formed before core formation, its composition would be even more primitive and neon solubility even lower. One alternative model is that of solar wind implantation (Trieloff *et al.*, 2000; Raquin and Moreira, 2009; Péron *et al.*, 2017), in which pre-planetary dust is irradiated by solar wind, enriching the embryos in $H_2$, He, O, C and Ne.

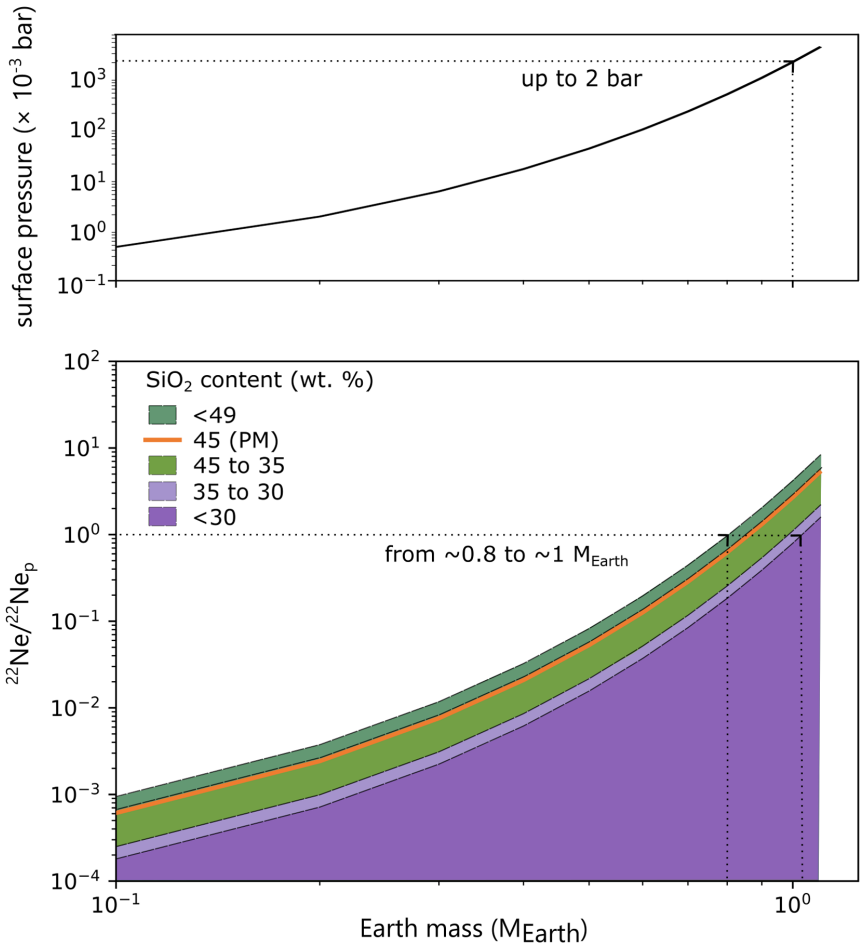


**Figure 2** **(a)** The surface pressure estimation follows the Jaupart *et al.* (2017) accretion model for a 10 Myr degassing period for the nebula. **(b)** For a given surface pressure, the $^{22}$Ne content relative to the primitive estimation ($^{22}Ne_p$) varies according to the solubility value applied; an embryo with over 0.8 $M_{Earth}$ is necessary to reach the primitive $^{22}$Ne content. PM = theoretical value obtained from Equation 1.

## Conclusion

Neon solubility decreases in approximately one order of magnitude between 49 and 30 wt. % $SiO_2$ ($3.4 \times 10^{-4}$ to $6.5 \times 10^{-5}$ $cm^3$ STP $g^{-1}$ $bar^{-1}$, respectively), supporting what has been previously shown in the literature for rhyolitic and basaltic composition experiments (*e.g.*, Carroll *et al.*, 1994). Our results allowed us to update the Jaupart *et al.* (2017) accretion model and show that dissolution of a primitive atmosphere into the magma ocean cannot account for the theoretical primitive mantle neon contents, requiring a body close to 1 $M_{Earth}$ to accumulate enough neon. Thus, alternative models are needed to explain the high $^{20}$Ne/$^{22}$Ne ratios found in deep mantle rocks.

## Acknowledgements

We thank R. Champallier, I. Di Carlo, and G. McGill for the technical support, and E. Núñez-Guerrero and R. Sauvalle for the scientific discussions and help with analyses. This research was funded by the ERC APATE project (DOI: 10.3030/101096688).

*Editor: Helen Williams*

## Additional Information

**Supplementary Information** accompanies this letter at https://www.geochemicalperspectivesletters.org/article2520.



**Cite this letter as:** Cardoso, C.D., Moreira, M., Scaillet, B. (2025) Solar neon dissolution into an ultramafic magma ocean. *Geochem. Persp. Let.* 35, 31–35. https://doi.org/10.7185/geochemlet.2520

## References

Albarède, F. (1996) Introduction to geochemical modeling. *Cambridge University Press*, 563pp. https://doi.org/10.1017/CBO9780511622960

Allègre, C. J., Staudacher, T., Sarda, P. (1986) Rare gas systematics: formation of the atmosphere, evolution and structure of the Earth's mantle. *Earth and Planetary Science Letters* 81, 127–150. https://doi.org/10.1016/0012-821X(87)90151-8

Carroll, M.R., Draper, D.S., Brooker, R.A., Kelley, S. (1994) Noble Gas Solubilities in Melts and Crystals. In: Matsuda, JI. (Ed.) *Noble Gas Geochemistry and Cosmochemistry*, Terra Scientific, Tokyo, Japan, 325–341.

Carroll, M.R., Stolper, E.M. (1993) Noble gas solubilities in silicate melts and glasses: New experimental results for argon and the relationship between

solubility and ionic porosity. *Geochimica et Cosmochimica Acta* 57, 5039–5051. https://doi.org/10.1016/0016-7037(93)90606-W

Di Carlo, I.D.A., Pichavant, M., Rotolo, S.G., Scaillet, B. (2006) Experimental crystallization of a high-K arc basalt: the golden pumice, Stromboli volcano (Italy). *Journal of Petrology* 47, 1317–1343. https://doi.org/10.1093/petrology/egl011

Doremus, R.H. (1966) Physical Solubility of Gases in Fused Silica. *Journal of the American Ceramic Society* 49, 461–462. https://doi.org/10.1111/j.1151-2916.1966.tb13299.x

Ercolano, B., Pascucci, I. (2017) The dispersal of planet-forming discs: Theory confronts observations. *Royal Society Open Science* 4, 170114. https://doi.org/10.1098/rsos.170114

Halliday, A., RehkZmper, M., Lee, D.-C., Yi, W. (1996) Early evolution of the Earth and Moon: new constraints from Hf-W isotope geochemistry. *Earth and Planetary Science Letters* 142, 75–89. https://doi.org/10.1016/0012-821X(96)00096-9

Heber, V.S., Baur, H., Bochsler, P., McKeegan, K.D., Neugebauer, M., Reisenfeld, D.B., Wieler, R., Wiens, R. C. (2012) Isotopic mass fractionation of solar wind: Evidence from fast and slow solar wind collected by the genesis mission. *The Astrophysical Journal* 759, 121. https://doi.org/10.1088/0004-637X/759/2/121

Iacono-Marziano, G., Paonita, A., Rizzo, A., Scaillet, B., Gaillard, F. (2010) Noble gas solubilities in silicate melts: New experimental results and a comprehensive model of the effects of liquid composition, temperature and pressure. *Chemical Geology* 279, 145–157. https://doi.org/10.1016/j.chemgeo.2010.10.017

Jambon, A., Weber, H., Braun, O. (1986) Solubility of He, Ne, Ar, Kr and Xe in a basalt melt in the range 1250-1600°C. Geochemical implications. *Geochimica et Cosmochimica Acta* 50, 401–408. https://doi.org/10.1016/0016-7037(86)90193-6

Jaupart, E., Charnoz, S., Moreira, M. (2017) Primordial atmosphere incorporation in planetary embryos and the origin of Neon in terrestrial planets. *Icarus* 293, 199–205. https://doi.org/10.1016/j.icarus.2017.04.022

Kleine, T., Walker, R.J. (2017) Tungsten Isotopes in Planets. *Annual Review of Earth and Planetary Sciences* 45, 389–417. https://doi.org/10.1146/annurev-earth-063016-020037

Kurz, M.D., Jenkins, W.J., Hart, S.R. (1982) Helium isotopic systematics of oceanic islands and mantle heterogeneity. *Nature* 297, 43–47. https://doi.org/10.1038/297043a0

Lux, G. (1987) The behavior of noble gases in silicate liquids: Solution, diffusion, bubbles and surface effects, with applications to natural samples. *Geochimica et Cosmochimica Acta* 51, 1549–1560. https://doi.org/10.1016/0016-7037(87)90336-X

Lyubetskaya, T., Korenaga, J. (2007) Chemical composition of Earth's primitive mantle and its variance: 1. Method and results. *Journal of Geophysical Research: Solid Earth* 112, 1–21. https://doi.org/10.1029/2005JB004223

Mizuno, H., Nakazawa, K., Hayashi, C. (1980) Dissolution of the primordial rare gases into the molten Earth's material. *Earth and Planetary Science Letters* 50, 202–210. https://doi.org/10.1016/0012-821X(80)90131-4

Moreira, M.A., Kurz, M.D. (2013) Noble gases as tracers of mantle processes and magmatic degassing. In: Burnard, P. (Ed.) *The Noble Gases as Geochemical Tracers*, Springer Berlin, Heidelberg, 371–391. https://doi.org/10.1007/978-3-642-28836-4_12

Olson, P.L., Sharp, Z.D. (2019) Nebular atmosphere to magma ocean: A model for volatile capture during Earth accretion. *Physics of the Earth and Planetary Interiors* 294, 106294. https://doi.org/10.1016/j.pepi.2019.106294

Olson, P., Sharp, Z.D. (2018) Hydrogen and helium ingassing during terrestrial planet accretion. *Earth and Planetary Science Letters* 498, 418–426. https://doi.org/10.1016/j.epsl.2018.07.006

Péron, S., Moreira, M., Putlitz, B., Kurz, M.D. (2017) Solar wind implantation supplied light volatiles during the first stage of Earth accretion. *Geochemical Perspectives Letters* 3, 151–159. https://doi.org/10.7185/geochemlet.1718

Raquin, A., Moreira, M. (2009) Atmospheric $^{38}Ar/^{36}Ar$ in the mantle: Implications for the nature of the terrestrial parent bodies. *Earth and Planetary Science Letters* 287, 551–558. https://doi.org/10.1016/j.epsl.2009.09.003

Shackelford, J.F., Studt, P.L., Fulrath, R.M. (1972) Solubility of Gases in Glass. II. He, Ne, and $H_2$ in Fused Silica. *Journal of Applied Physics* 43, 1619–1626. https://doi.org/10.1063/1.1661371

Shibata, T., Takahashi, E., Matsuda, J.-I. (1998) Solubility of neon, argon, krypton, and xenon in binary and ternary silicate systems: A new view on noble gas solubility. *Geochimica et Cosmochimica Acta*, 62, 1241–1253. https://doi.org/10.1016/S0016-7037(98)00046-5

Trieloff, M., Kunz, J., Clague, D.A., Harrison, D., Allègre, C.J. (2000) The Nature of Pristine Noble Gases in Mantle Plumes. *Science* 288, 1036–1038. https://doi.org/10.1126/science.288.5468.1036

Walsh, K.J., Levison, H.F. (2016) Terrestrial planet formation from an annulus. *The Astronomical Journal* 152, 68. https://doi.org/10.3847/0004-6256/152/3/68

Williams, C.D., Mukhopadhyay, S. (2019) Capture of nebular gases during Earth's accretion is preserved in deep-mantle neon. *Nature* 565, 78–81. https://doi.org/10.1038/s41586-018-0771-1

Williams, J.P., Cieza, L.A. (2011) Protoplanetary Disks and Their Evolution. *Annual Review of Astronomy and Astrophysics* 49, 67–117. https://doi.org/10.1146/annurev-astro-081710-102548

Yin, Q., Jacobsen, S.B., Yamashita, K., Blichert-Toft, J., Télouk, P., Albarède, F. (2002) A short timescale for terrestrial planet formation from Hf-W chronometry of meteorites. *Nature* 418, 949–952. https://doi.org/10.1038/nature00995

Yokochi, R., Marty, B. (2004) A determination of the neon isotopic composition of the deep mantle. *Earth and Planetary Science Letters* 225, 77–88. https://doi.org/10.1016/j.epsl.2004.06.010